Biomaterials 212 (2019) 115–125

Contents lists available at ScienceDirect

Biomaterials

journal homepage: www.elsevier.com/locate/biomaterials

An on-chip model of protein paracellular and transcellular permeability in the microcirculation

Giovanni S. Offeddu[a], Kristina Haase[b], Mark R. Gillrie[a], Ran Li[a], Olga Morozova[c,d], Dean Hickman[d], Charles G. Knutson[d,**], Roger D. Kamm[a,b,*]

[a] Department of Biological Engineering, Massachusetts Institute of Technology, Cambridge, MA, USA
[b] Department of Mechanical Engineering, Massachusetts Institute of Technology, Cambridge, MA, USA
[c] Department of Molecular and Cellular Biology, Harvard University, Cambridge, MA, USA
[d] Amgen Research, Amgen Inc., 360 Binney Street, Cambridge, MA, USA

ARTICLE INFO

Keywords:
Organ-on-chip
Microfluidics
Trans-endothelial transport
Permeability
FcRn

ABSTRACT

Recent therapeutic success of large-molecule biologics has led to intense interest in assays to measure with precision their transport across the vascular endothelium and into the target tissue. Most current *in vitro* endothelial models show unrealistically large permeability coefficients due to a non-physiological paracellular transport. Thus, more advanced systems are required to better recapitulate and discern the important contribution of transcellular transport (transcytosis), particularly of pharmaceutically-relevant proteins. Here, a robust platform technology for the measurement of transport through a human endothelium is presented, which utilizes *in vitro* microvascular networks (MVNs). The self-assembled MVNs recapitulate the morphology and junctional complexity of *in vivo* capillaries, and express key endothelial vesicular transport proteins. This results in measured permeabilities to large molecules comparable to those observed *in vivo,* which are orders of magnitude lower than those measured in transwells. The permeability of albumin and immunoglobulin G (IgG), biopharmaceutically-relevant proteins, is shown to occur primarily via transcytosis, with passage of IgG regulated by the receptor FcRn. The physiological relevance of the MVNs make it a valuable tool to assess the distribution of biopharmaceuticals into tissues, and may be used to prioritize candidate molecules from this increasingly important class of therapeutics.

1. Introduction

Therapeutic recombinant proteins and antibodies, so-called biopharmaceuticals or biologics, have revolutionized the way we address disease [1]. These large (> 10 kDa) molecules are designed with moieties that target disease-specific antigens, offering greater selectivity compared to small (< 1 kDa) molecule therapeutics [2]. Unlike small molecules, biopharmaceuticals are often recognized by the host body and re-circulated to prolong half-life. Continuous developments in biotechnological design and manufacturing have allowed for mass production of these complex molecules, providing greater access to patients. The ever-increasing number of therapies available in the clinic now includes monoclonal antibodies targeting TNFα in autoimmune disease [3] and PD-L1 checkpoint inhibitors in cancer [4]. Owing to an overall successful track-record, biopharmaceuticals have experienced tremendous growth in development and application, with projected US revenues in excess of 264 billion dollars in 2018 alone [5].

The therapeutic efficacy of biopharmaceuticals critically depends on their ability to reach the intended target *in vivo*. To leave the circulation and enter the target microenvironment, molecules must cross the capillary endothelium, the primary barrier to biodistribution. Endothelial barrier function is determined by paracellular permeability, controlled by cell-cell junctions, and transcellular permeability, mediated through vesicular transport [6]. While small molecules can often pass between endothelial cells by passive paracellular transport, proteins such as biopharmaceuticals are usually too large to do so [7]. Transport across the endothelium for these large molecules, therefore, is diminished and may only occur through active transcellular mechanisms. Since the endothelium hinders the access of biopharmaceuticals to their target site, ultimately limiting the therapeutic efficacy of these molecules, an understanding of transendothelial transport via these two distinct pathways is key to develop molecules with enhanced distribution

* Corresponding author. Department of Biological Engineering, Massachusetts Institute of Technology, NE47-318, Cambridge, MA, USA.
** Corresponding author. Amgen Inc., 360 Binney Street, Cambridge, MA, USA.
E-mail addresses: charlie.knutson@amgen.com (C.G. Knutson), rdkamm@mit.edu (R.D. Kamm).

https://doi.org/10.1016/j.biomaterials.2019.05.022
Received 3 January 2019; Received in revised form 23 April 2019; Accepted 10 May 2019
Available online 13 May 2019
0142-9612/

profiles.

The ability of specific biotherapeutics to cross the human endothelium is currently evaluated using *in vitro* or *in vivo* methodologies [8]. Standard *in vitro* models make use of human endothelial cells arranged within a transwell system in a monolayer. This system allows for direct measurement of protein concentration over time in both compartments, hence of solute flux. However, the two-dimensional (2D) geometry in which the endothelial cells are arranged fails to replicate the three-dimensional (3D) structure of the human capillary bed and its complex microenvironment involving interactions between multiple different cell types. As a result, the measurement may not be physiologically-relevant and often produce permeabilities much larger than those observed *in vivo* [9]. Alternatively, animal models can be used to make intravital measurements of solute distribution. While these models possess an intrinsic physiological complexity, measurements made in small animals may not be clinically translatable to transport in the human circulatory system [10]. These models are inherently low throughput, and increase our reliance on animal testing. In addition, spatiotemporal resolution for such measurements is greatly diminished by difficulties in imaging thick, live specimens. Thus, the techniques currently available to measure biopharmaceutical transendothelial distribution are limited.

A number of research groups have attempted to generate a functional human endothelium within microfluidic devices (reviewed in Ref. [9]). However, the characterization of protein transcytosis was not the object of those studies, which limited their investigation to the measurement of baseline paracellular permeability. Here, we report on a method to conduct physiologically-relevant measurements of protein transendothelial transport without sacrificing spatiotemporal resolution, by using 3D self-assembled human microvascular networks (MVNs) within microfluidic devices. We show that the endothelial permeability values of large molecules are within the range observed *in vivo*, orders of magnitude smaller than those measured in transwell assays. Further, this methodology was used to investigate the neonatal Fc receptor, FcRn, which based on previous *in vivo* and 2D endothelial permeability studies has a controversial role in the transcytosis of albumin and immunoglobulin G (IgG), plasma proteins on which most biotherapeutics are structurally based [11].

2. Materials and methods

2.1. Microfluidic device fabrication

A multi-device mold was fabricated by laser cutting 0.5 mm thick poly (methyl methacrylate) sheets (Astra products, US) on an Epilog Fusion 40 machine, producing devices with 3 channels (3 mm wide each). The central gel channel is approximately 20 mm long, from gel port to gel port. The microfluidic device makes use of a guide-edge ($\approx$1/3 of the device height) to ensure gel containment within the central channel by surface tension upon injection. A “raster” pattern was used at 20% laser power to generate the guide-edge, which resulted in a partial wall of approximately 200 μm between channels. Laser-cut pieces were bonded to a larger sheet of acrylic (McMaster Carr, US) and inverse molds were generated using polydimethylsiloxane (PDMS, Dow Corning Sylgard 184, Ellsworth Adhesives, US). PDMS devices were cut, punched, sterilized by autoclave (20 min), and finally bonded to clean #1 glass coverslips before further baking at 70 °C.

2.2. MVN formation

Human Umbilical Vein Endothelial Cells (HUVECs) and HUVECs GFP were purchased from Angio-Proteomie, US, and normal Human Lung Fibroblasts (nHLFs) from Lonza, US. They were cultured on collagen-coated flasks (Corning, US) in a controlled 5% CO_2 atmosphere at 37 °C, with Lonza EGM-2MV and FGM-2, respectively, and frozen following four passages. After thawing and re-plating on uncoated flasks, cells were seeded into devices in fibrin gel as previously described [12], at a final concentration of 5 million mL^{-1} and 2.5 million mL^{-1}, respectively. Excess HUVECs were re-plated and kept for use in the monolayer. The MVNs were cultured for seven days in EGM-2MV, replaced daily; on day four, 1.5 million cells per mL of EGM-2V were added to the emptied media channels, 100 μL per channel, where over the remaining three days of culture they formed a monolayer on the fibrin gel surface.

2.3. Permeability measurement and reagents

All solutes tested for endothelial permeability were obtained conjugated to fluorescein isothiocyanate (FITC). Dextrans were purchased from Sigma Aldrich, US (46944, FD40, FD70, 46946, FD500S, 74187, 75005) and so was human serum IgG (F9636). Human serum albumin was purchased from Abcam (ab8030). Dynamic light scattering and zeta potential measurements for the solutes were performed on a Malvern Zeta-sizer. Permeability was tested, unless otherwise stated in the text, by dissolving each solute at a concentration of 0.1 mg mL^{-1} in EGM-2MV. The small protein concentration, and consistent dextran concentration, was chosen so to induce little oncotic pressure (less than 5 Pa for both albumin and IgG [13]). All permeability measurements were performed with interal hydrostatic pressures kept below 50 Pa, in a range where no solute filtration should take place [14]. Perfusion of the MVNs was performed by first emptying one media channel and filling it with fresh, solute-containing media, after which the other media channel was also emptied and the fluid left to perfuse across the network over approximately 2 min, before adding to the second media channel additional solute-containing media to equilibrate pressures. For the vascular endothelial growth factor (VEGF) experiment, exogenous human VEGF 165 (Peprotech, US) was added at a concentration of 50 ng mL^{-1} to complete EGM and incubated in the device under a slight pressure gradient of 50 Pa for 0.5 h at 37 °C and 5% CO_2. Imaging of the perfused network was performed on an Olympus FV1000 confocal microscope with custom enclosure for temperature and atmosphere control. Stacks were collected using a 10X objective at a resolution of 800×800 pixels every 12 min, using a *z*-spacing of 5 μm and a minimum stack size of 20 slices. Reconstruction of the geometry was conducted using ImageJ, FIJI distribution [15], by automatic thresholding and segmentation of the solute signal. The average intensity in the vascular and matrix compartments were used to measure the permeability coefficient, *P*, as the resistance per endothelial surface area, *SA*, offered by the endothelium against the solute flux J_s (units: mol s^{-1}), which is driven by a transendothelial concentration difference Δc [16]:

$$P = \frac{J_S}{SA\ \Delta c} \quad \text{(Eq. 1)}$$

which takes the expanded form:

$$P = \frac{V_m}{SA\ \Delta I}\frac{\Delta I_m}{t} \quad \text{(Eq. 2)}$$

where t is the time over which transport is assessed and $\Delta I_m = I_{m,2} - I_{m,1}$ is the increase in mean fluorescence intensity, assumed linearly proportional to solute concentration, in the matrix of volume V_m between time-points and $\Delta I_m = I_{v,1} - I_{m,1}$ the difference in intensity, therefore solute concentration, between the vasculature and matrix at the start of the measurement. The average matrix intensity after $t = 12$ min, $I_{m,2}$, was normalized to account for the systematic decrease in intensity due to bleaching and microscope drift, so that:

$$I^*_{m,2} = I_{m,2}\frac{I_{v,1}}{I_{v,2}} \quad \text{(Eq. 3)}$$

where I_v is the average intensity in the vascular space at the first and second time-point, as indicated by the respective subscripts. Transwell cell culture and permeability measurements were conducted using

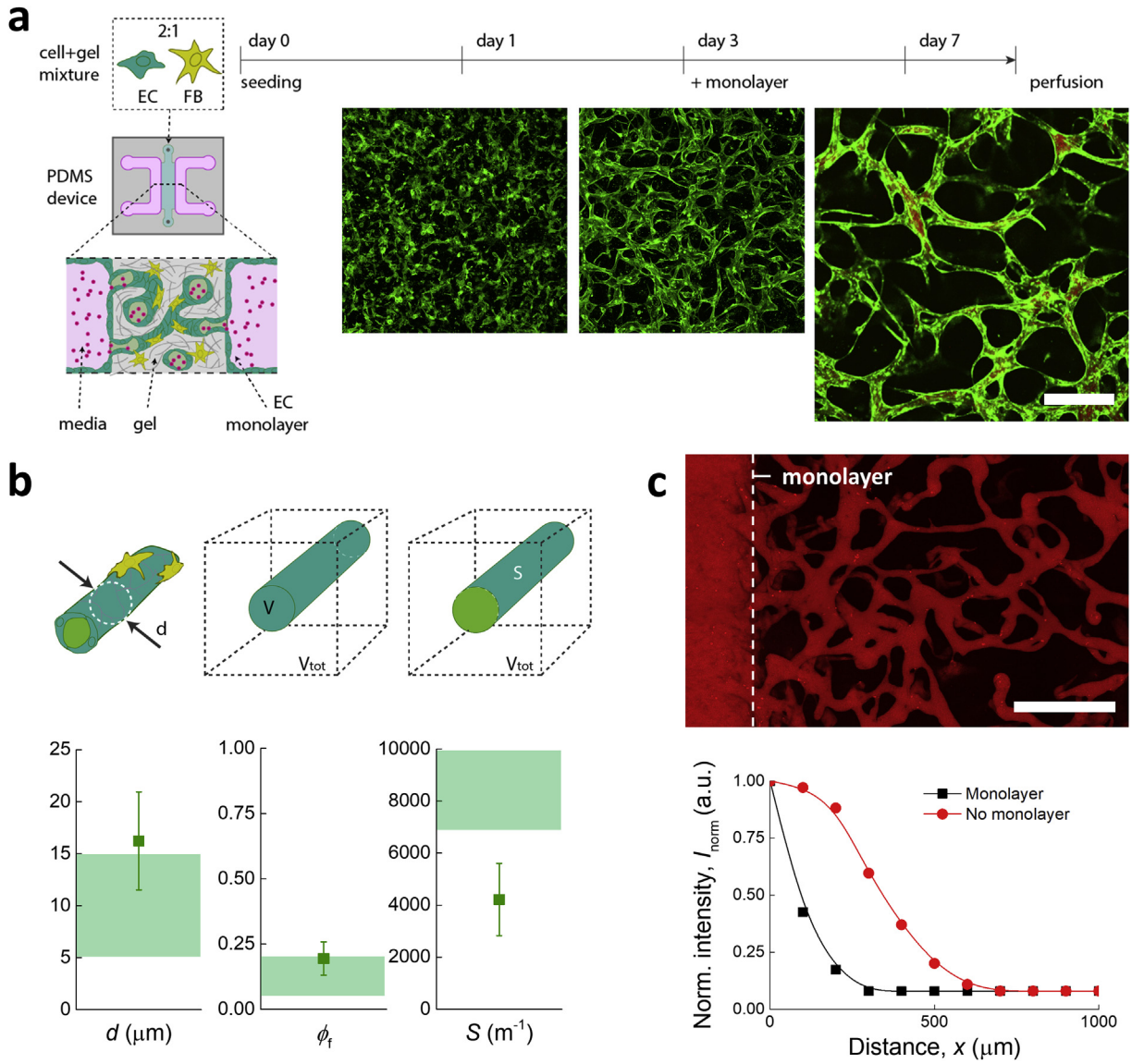

Fig. 1. MVNs self-assemble into a continuous, perfusable endothelium suitable for transport measurements. (**a**) Schematic diagram of the MVNs microfluidic device (left) and confocal images of the formation of perfusable MVNs over seven days of co-culture of endothelial cells (EC) and fibroblasts (FB) in fibrin gel within the device (right; green = HUVECs GFP, red = dextran; the scale bar is 100 μm). (**b**) Comparison of MVNs morphological parameters (data points and error bars indicate average and standard deviation, respectively; n = 15) with the range expected *in vivo* (shaded area, references provided in the text). (**c**) HUVECs monolayer separating media and gel channels prevents direct solute diffusion through the matrix as visualized from a collapsed confocal microscopy image of 70 kDa dextran (red) perfusing the MVNs (scale bar = 200 μm) and an example solute intensity profile within the matrix as a function of distance from the media channel after the typical measurement time (12 min) in the presence and absence of a monolayer along the gel channel. (For interpretation of the references to color in this figure legend, the reader is referred to the Web version of this article.)

collagen-coated well-plate inserts (354482, Corning, US) according to the manufacturer's protocol. In the case of co-culture, endothelial cells were seeded in the inserts, and fibroblasts were seeded at the bottom of the lower wells. Fluorescence intensities of the fluids collected from the two reservoirs were measured on a Cytation 5 fluorescence plate reader (BioTek, US), at excitation/emission wavelengths of 490/530, and Eq. (2) applied to measure transwell permeability.

2.4. Antibodies, glycocalyx staining, and colocalization analysis

Immunofluorescence staining of endothelial junctions was performed in fixed MVNs using a polyclonal antibody against VE-cadherin (ALX-210-232, Enzo Lifesciences) and a monoclonal ZO-1 antibody (33–91100, Invitrogen). The glycocalyx was live-stained for 30 min using FITC-conjugated lectin from triticum vulgaris (L4895, Sigma, US), followed by washing of the MVN lumens with fresh media. The pixel resolution for the glycocalyx thickness measurement was 0.97 μm. All 2D cell imaging was conducted on HUVECs plated on collagen-coated substrates (Corning, US). Colocalization analysis was performed on histological sections of the MVNs with Cell Signalling Technologies CAV1 (3238S), Clathrin (2410S), RAB5 (2143S), and LAMP1 (9091S) antibodies, and R&D systems FcRN antibody (8639). A 60X oil objective was used on the same confocal microscope mentioned above, with a pixel resolution of 2048 × 2048. The analysis was automatically performed through the ImageJ Colocalization function, after manually highlighting lumens.

2.5. Investigation of FcRn-dependent transcytosis

The pH of EGM-2MV was adjusted drop-wise to a value of six using

hydrochloric acid. IgG was perfused in pH 6 media without prior pre-treatment so not to alter the matrix pH. Bafilomycin A1 was purchased from Tocris, US (1334), and dissolved in DMSO. Dilution in EGM-2MV produced a final concentration of 1 μM bafilomycin and 0.2% DMSO. The latter concentration was produced in the controls for the experiment, and samples were pre-treated for 30 min (with bafilomycin or without) before perfusion of IgG in their respective media.

Knockdown was performed as per the manufacturer's instructions (Qiagen) with slight modifications as detailed. At the time of transfection, the medium from the MVNs was aspirated and replaced with transfection mixture of 2.5 μl HiPerfect (Qiagen), and 50 nM siRNA for FcRn (siRNA 1, 2 or both, Qiagen) or AllStars Negative Control (Qiagen) added in 100 μl of OptiMEM. At 4 h after transfection, 0.1 mL of endothelial media was added to each well and changed daily thereafter. Transfected cells were used in permeability experiments on day 9, 48 h after transfection. Knockdown of FcRn was confirmed by flow cytometry analysis of HUVECs seeded at 5×10^5 cells/well of six-well plates and transfected 24 h later at ~70% confluence as above. FcRn was detected on HUVECs 48 h post-transfection using intracellular staining reagent (BioLegend) with FcRn antibody (R&D, 5 μg/mL) or Isotype control (R&D, 5 μg/mL) and goat anti-mouse Alexa-568 (Invitrogen). Analysis was performed on a Becton Dickinson LSR II flow cytometer at the MIT Koch Institute Flow Cytometry Core Lab.

2.6. Scanning electron microscopy (SEM)

Specimens were fixed with 0.15 M Cocadylate buffer with 2% paraformaldehyde and 2% glutaraldehyde. For electron microscopy imaging, samples were stained with the rOTO method (2% osmium in 1.5% ferrocyanide for 1 h followed by 1% thiocarbohydrazyde for 20 min and 2% osmium for 30 min), dehydrated in ethanol and acetonitrile, and embedded in embed 812 epoxy resin. Ultrathin sections were collected at 40 nm with a microtome, and imaged with a Sigma scanning electron microscope (Carl Zeiss).

2.7. Statistical analysis

Transwell permeability measurements were performed in three repeats per solute. MVNs permeability measurements were performed in three devices from three separate biological repeats, each of which was used for three separate measurements (*z*-stacks), except in the case of the siRNA experiment, where only two repeats were done due to the presence of multiple controls. All data representation details are provided in the figure captions, and single data points are reported where clarity of the figure can be maintained. Statistical significance was assessed using student's t-tests performed with the software OriginPro 2016, where differences at $p < 0.05$ were taken as significant (*, $p < 0.001$ **, $p < 0.0001$ ***, $p < 0.00001$ ****).

3. Results

3.1. Fabrication and perfusion of MVN devices

Functional 3D MVNs to study endothelial barrier function in the presence of extracellular matrix and stromal cells are generated by co-culturing HUVECs and nHLF over seven days within a fibrin hydrogel (Fig. 1a). Cells are mixed with the hydrogel precursors, fibrinogen and thrombin, and injected together into the central channel of a PDMS three-channel microfluidic device, where fibrin quickly polymerizes suspending cells in a 3D matrix. The side channels of the devices are then filled with cell culture medium. In this co-culture environment, HUVECs undergo a process mimicking vasculogenesis whereby they form endothelial connections, branch and anastomose, bridging the gap between the two media channels with fully connected lumens after five to seven days.

The morphology of the self-assembled 3D MVNs resembles that of mammalian capillary beds (Fig. 1b). The microvessels have an average diameter $d \approx 20$ μm, close to the physiological human range for capillaries (5–15 μm [17]). Due to a small amount of cell sedimentation during fibrin polymerization, larger vessels may be observed at the bottom of the device. The volumetric density of the networks, φ_v, defined as the ratio between MVNs' and total volume (V_v/V_{tot}), is approximately 20% and within the range expected *in vivo* (8–21% [18,19]), while the vascular surface area per volume available for transport, $S = S_v/V_{tot}$, is close in magnitude to the range expected for tissues like the human brain ($4500\ m^{-1}$ compared to $7000\ m^{-1}$ [20]). The morphological similarities to the normal human endothelium include, most importantly, the presence of open lumens, which can be perfused from the side channels with any molecule dissolved in the cell culture medium or other liquid.

To ensure all transport into the extracellular matrix surrounding the vasculature takes place across the endothelium, the sides of the central gel channel are coated with HUVECs on day four. This configuration allows for growth of a continuous endothelial monolayer lining the large media channels, seamlessly integrating with the endothelial cells of the MVNs within the gel (Fig. 1c). The presence of this monolayer prevents solute diffusion from the media channels directly into the gel matrix over the time of the experiment, ensuring accurate transendothelial transport measurements.

3.2. Measurement of physiologically-relevant endothelial permeability

In transwells, the most commonly used *in vitro* endothelial barrier models, solute flux occurs across a 2D surface, between the fluids contained in the two reservoirs separated by an endothelial monolayer grown in isolation on a rigid porous membrane. In contrast, the endothelium in the MVNs system adopts a more physiologic 3D morphology (Fig. 2a), and the flux takes place from the lumens into an extra-cellular matrix.

To establish the baseline barrier function of the MVNs to large molecules we first made use of 4–500 kDa dextrans, model molecules that have been used in numerous *in vitro* and *in vivo* studies (Fig. 2b). To test whether the 3D MVNs provided improved barrier function that is reflective of *in vivo* values, we compare co-culture of HUVECs and fibroblasts in our 3D system to co-culture in a standard transwell assay. For both systems, when the molecular weight, hence size (Fig. 2c), of the dextrans increases, the permeability decreases ($p < 0.01$ in both cases). The decrease in permeability observed follows an exponential decay with molecular weight ($R^2 = 0.97$ in both cases, Supplementary Fig. 1a), consistent with diffusion of solutes through pores [21]. However, the decrease is faster for the 3D MVNs compared to the 2D transwells ($\sigma = 19.92$ and 12.74, respectively, where $P \propto \exp(-M_w/\sigma)$) suggesting that the transwell monolayer is a less size-selective barrier. Consistently, the permeability of the 3D MVNs is two orders of magnitude smaller than for the same cells in transwells ($10^{-8}\ cm\ s^{-1}$ versus $10^{-6}\ cm\ s^{-1}$). When compared to dextran permeability values reported previously, our transwell results compare well in terms of order of magnitude with other transwell endothelial monolayer measurements [22,23], including values for HUVECs [24,25]. Instead, the MVNs show values that fit into the much lower permeability range reported for measurements performed in animal models, including values for the brain, lung and muscle [26,27].

The striking difference in permeability to dextrans between the two systems may derive from the dissimilarities between the physicochemical microenvironments in which the endothelial cells reside. In the MVN system, endothelial cells are attached to a compliant hydrogel matrix; instead, the membrane on which HUVECs reside in the transwells possibly provides a stiffer substrate, which could affect barrier function [28]. Co-culture of endothelial cells with stromal cells has been shown to increase barrier function, *e.g.* in the case of human brain endothelial cells with astrocytes [29]. Here, paracrine signalling from fibroblasts does not appear, alone, to alter HUVECs barrier function, as

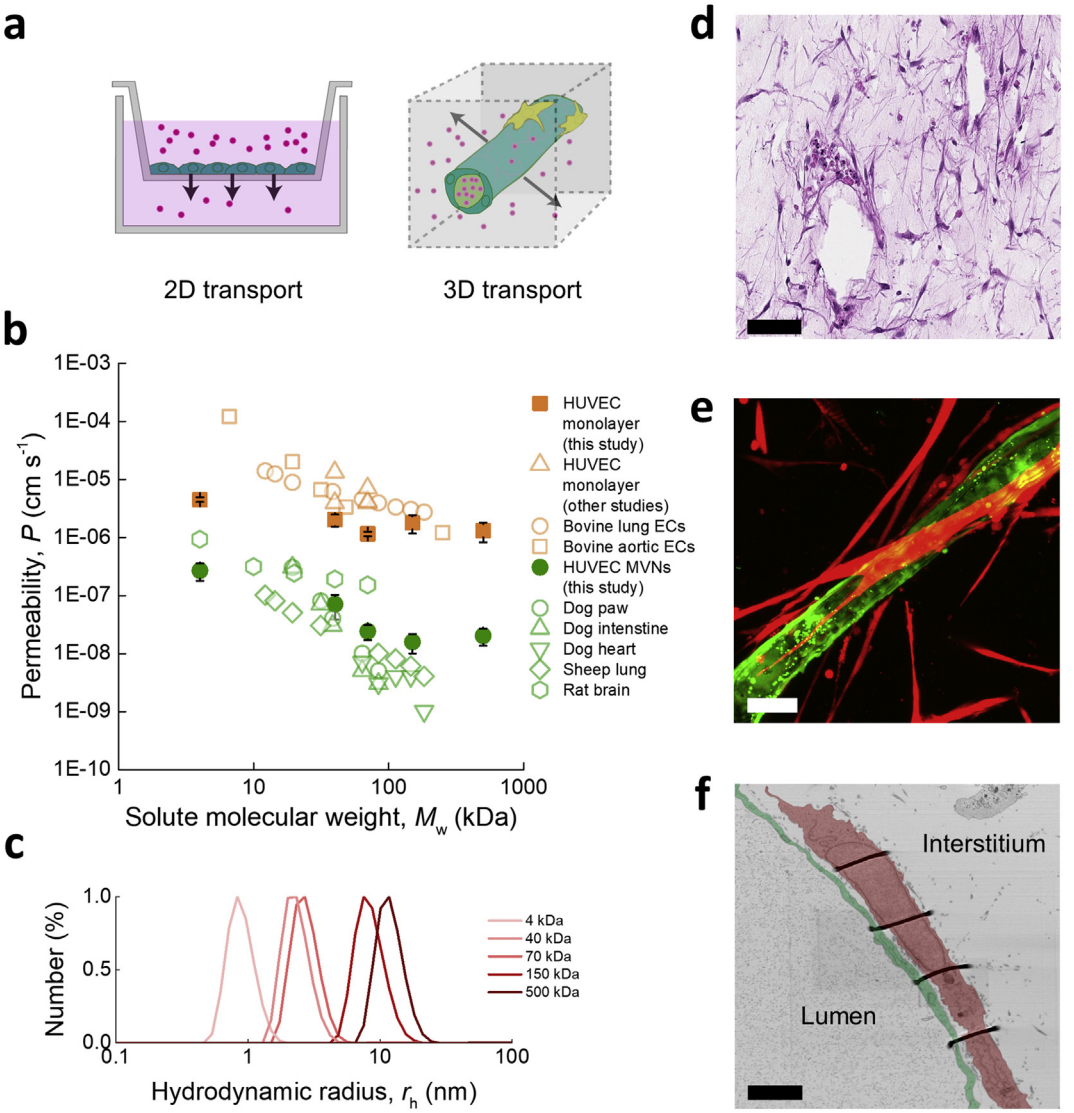

Fig. 2. MVNs outperform transwell systems in terms of physiological relevance of permeability to dextran. (**a**) Comparison between the 2D and 3D model of transport in the transwell and MVN systems, respectively. (**b**) Permeability of HUVEC monolayers (filled squares) and MVNs (filled circles) compared to other *in vitro* and *in vivo* measurements reported in the literature (references provided in the text). The data points and error bars represent the average and standard deviation; $n = 3$ for transwell measurements, 3×3 measurements for the MVNs. (**c**) Dynamic light scattering size distributions of dextran as a function of molecular weight. (**d**) H&E stain of a MVN section showing two lumens and the surrounding fibroblast-rich matrix. The scale bar is 40 μm. (**e**) Confocal microscopy image of a MVN capillary (HUVECs GFP) in direct contact with fibroblasts (RFP). The scale bar is 20 μm. (**f**) False-color SEM image of fibroblast (red)-coated MVN endothelium (green). The scale bar is 1 μm. (For interpretation of the references to color in this figure legend, the reader is referred to the Web version of this article.)

the transwell values for dextran permeability are comparable with or without fibroblast co-culture in the bottom reservoir (Supplementary Fig. 1b). Nevertheless, in the MVN system fibroblasts may provide additional cues to the endothelial cells, as they are often seen to be in direct physical contact by lining the microvessels on the basal side (Fig. 2d–f).

While size evidently affects the capacity of solutes to cross the endothelium, other molecular physicochemical properties also impact transport. In particular, it has been shown that the charge of solutes determines capillary permeability *in vivo* and, as a result, solute distribution to tumors [30]. Here, we test the MVNs permeability of dextrans of the same molecular weight but varying charge (positive or negative), as confirmed by zeta-potential measurements (Fig. 3a). The MVNs permeability to positively-charged dextran is significantly higher than to the neutral dextran of same size (Fig. 3b), similarly to what has been previously reported [30]. At the same time, the permeability to negatively-charged dextran is, on average, lower than to the neutral molecule. These findings are in agreement with the MVNs expression of a functional, negatively-charged glycocalyx (Fig. 3c), with a thickness of the order of 1 μm (Fig. 3d), as recently reported for *in vivo* capillaries [31]. Significantly, while expression of a glycocalyx is also observed in the transwell system, the solute charge-dependent permeability seen for the MVNs is not observed in the transwell systems (Supplementary Fig. 2).

The dissimilarity in permeability between MVNs and transwell monolayers also extends to proteins. The magnitude of transendothelial transport for human serum albumin and IgG is two orders of magnitude smaller in the MVNs, irrespective of transwell co-culture with fibroblasts (Fig. 4a and b). Similar to the dextrans, protein permeability values measured in the MVNs are within the range of those measured *in vivo*, on the order of 10^{-8} cm s^{-1} [27,32]. The reason for this dramatic difference between 2D and 3D permeability measurements may be due to discontinuities present at endothelial junctions in 2D (Fig. 4c), although other factors may contribute, such as alterations in glycocalyx

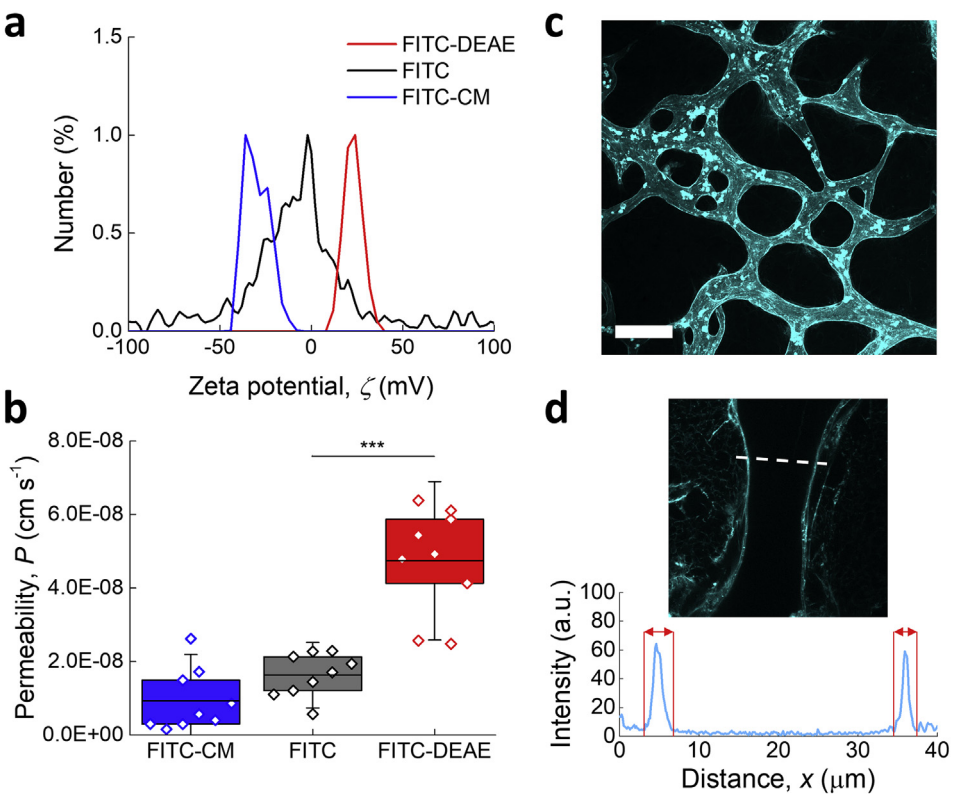

Fig. 3. MVNs express a functional glycocalyx. (**a**) Zeta potential measurement of 150 kDa dextran as a function of charged side-group. (**b**) MVN permeability to 150 kDa dextran is impacted by charged side-group of the solute. The box and whisker plot represents the outliers that fall within the 25th and 57th percentile; statistical significance asserted by student's t-test, *, $p < 0.001$ **, $p < 0.0001$ ***, $p < 0.00001$ ****. (**c**) Collapsed confocal image of glycocalyx (lectin live stain, cyan). The scale bar is 100 μm. (**d**) Confocal microscopy image of capillary section and depiction of glycocalyx thickness. (For interpretation of the references to color in this figure legend, the reader is referred to the Web version of this article.)

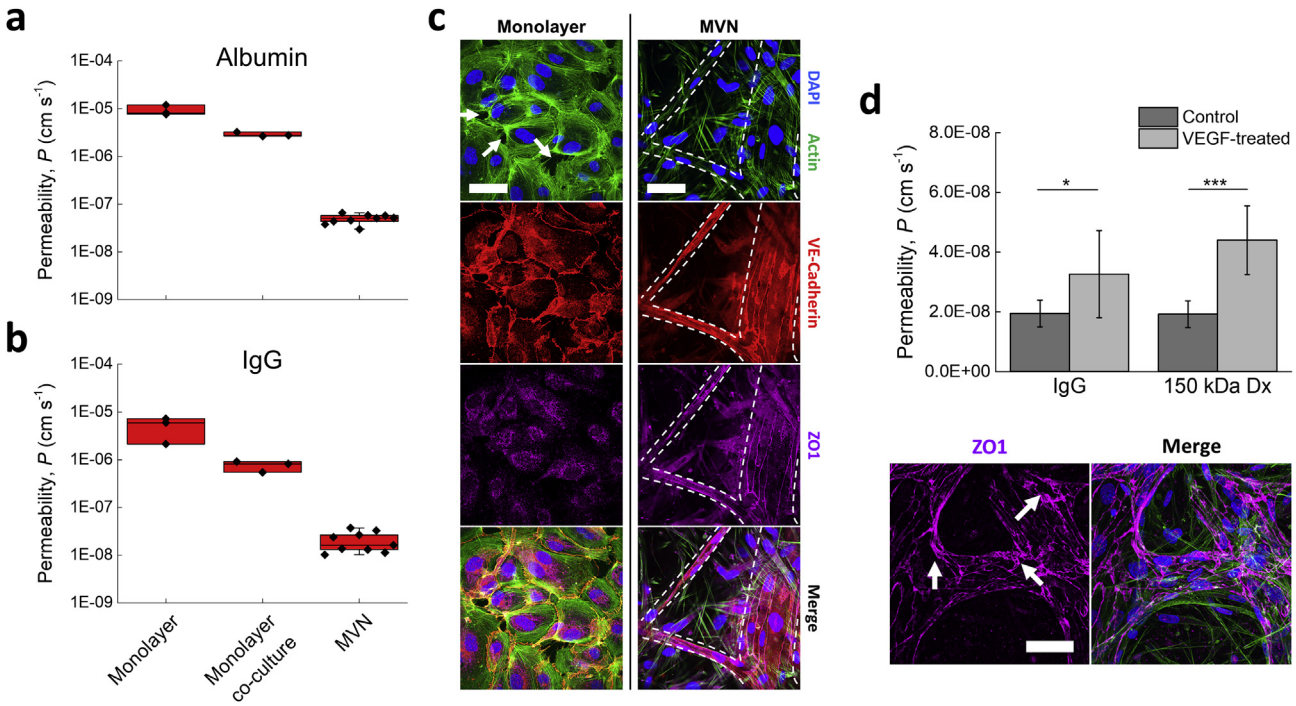

Fig. 4. Protein permeability through MVNs is reduced due to continuous endothelial junctions. Transwell permeability of endothelial cells with and without co-culture with fibroblasts compared to MVNs in the case of human serum (**a**) albumin and (**b**) IgG. The box and whisker plot represents the outliers that fall within the 25th and 57th percentile; $n = 3$ for transwell measurements, 3×3 measurements for the MVNs. (**c**) Immunofluorescence staining of endothelial adherens (VE-Cadherin) and tight (ZO1) junctions for cells plated in 2D and cells forming the MVNs. The arrows point at gaps in the 2D monolayer. The scale bars are 50 μm. (**d**) MVNs permeability to IgG and 150 kDa dextran as a result of pre-treatment with VEGF. Data plotted as average and standard deviation; $n = 3 \times 3$ measurements, statistical significance assessed by student's t-test, *, $p < 0.001$ **, $p < 0.0001$ ***, $p < 0.00001$ ****. Immunofluorescence staining for tight junctions reveals signs of junction unravelling in the presence of VEGF, but not gaps as seen in the monolayers.

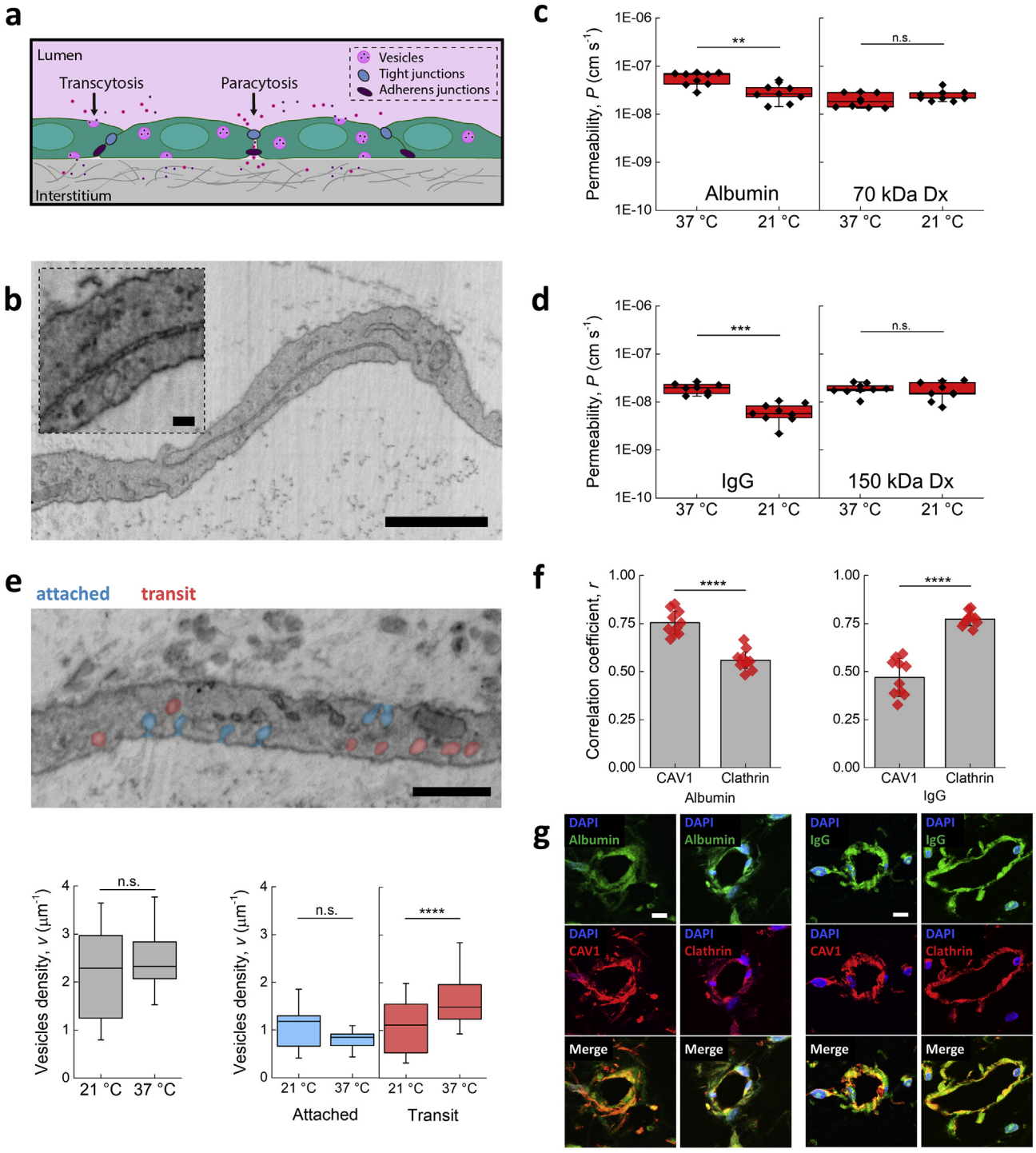

Fig. 5. MVN permeability to albumin and IgG depends on transcytosis. (**a**) Schematic diagram of different modes of transport across endothelia. (**b**) SEM image of MVN endothelial junction. The scale bar is 1 μm, 50 nm in the inset. The impact of temperature on MVN permeability to (**c**) albumin and 70 kDa dextran, and (**d**) IgG and 150 kDa dextran. The box and whisker plot represents the outliers that fall within the 25th and 57th percentile; $n = 3 \times 3$ measurements. (**e**) Analysis of vesicular transport through counting of vesicles attached to the cell membrane or in transit as a function of temperature. Box and whisker plot as above; $n > 300$ vesicles per condition. The scale bar is 500 nm (**f**) Co-localization analysis of albumin and IgG with markers for caveolae (CAV1) and clathrin-coated pits (clathrin). The scale bars are 10 μm. Statistical significance assessed for all data portrayed by student's t-test, *, $p < 0.001$ **, $p < 0.0001$ ***, $p < 0.00001$ ****.

and basement membrane structure arising from the dissimilarities in microenvironment considered above. Our results suggest that the 3D MVNs likely present selective improvements in paracellular barrier function that also affect large proteins like albumin and IgG. The high permeabilities observed in transwell systems, on the order of 10^{-6} to 10^{-5} cm s^{-1}, far exceed the values measured for a leaky endothelium in the MVNs, demonstrated by treatment of the MVNs with VEGF (Fig. 4d). Through the recapitulation of a physiological endothelial morphology and physicochemical microenvironment, the MVNs clearly outperform conventional transwell systems in exhibiting more physiologically-relevant values of permeability.

3.3. Determination of mode of transport

Solutes cross the endothelium by two mechanisms (Fig. 5a): Paracytosis through the junctions between endothelial cells, which is driven by diffusion and convection, or transcytosis through endothelial cells, often involving specific recognition and active cellular transport through vesicles [6]. Large proteins may be prevented from crossing the endothelium entirely by paracytosis, as their size could hinder their passage between endothelial junctions, or even through the glycocalyx mesh [33]. Similar to capillaries *in vivo* [34], the MVNs show junctions with clefts of approximately 10 nm, here observed to be bridged and become smaller in the presence of, what are most likely, adherens or tight junctions (Fig. 5b). We, therefore, expect the 3D MVNs to recapitulate a physiologically-relevant cell junction barrier to albumin and IgG.

A simple way to differentiate between different modes of transendothelial transport is by modulating the temperature of the endothelium, since at lower temperature vesicles are increasingly prevented from budding away from the cell membrane and transit through the cytoplasm [35], thereby reducing transcytosis. In the MVNs, when temperature is lowered from physiological (37 °C) to room temperature (21 °C), the average permeability drops by approximately 47% for albumin and 67% for IgG (Fig. 5c and d). At the same time, the permeability to dextrans of similar molecular weight, 70 kDa and 150 kDa, respectively, does not change. In the analysis described, all room temperature results were adjusted for the change in viscosity with temperature affecting diffusion, as per the Stokes-Einstein equation (calculated factor = 1.48) [21].

The decreased permeability of albumin and IgG as the temperature is lowered suggests that their transport occurs at least in large part through transcytosis, while the constant dextrans permeability irrespective of temperature implies paracellular crossing of the endothelium. The temperature-dependent change in vesicular transport in the MVNs can be visualized through electron microscopy (Fig. 5e). The overall number of vesicles per length of endothelium does not change with temperature, but the number of vesicles in transit through the cytoplasm decreases with decreasing temperature. That is, the number of vesicles attached to the cell membrane is larger at lower temperatures, consistent with decreased protein transcytosis.

Vesicular transport across the endothelium occurs through either plasmalemmal caveolae or clathrin-coated pits [6], corresponding to different protein receptors. Co-localization analysis in the MVNs (Fig. 5f) shows that albumin is significantly more localized in caveolae, in agreement with the presence of gp60, a key receptor for albumin, in these vesicles [36]. In contrast, IgG is significantly more localized in clathrin-coated pits. Interestingly, 2D-cultured monolayers of HUVECs demonstrate the same trend for albumin, yet IgG does not appear to be significantly localized in either type of vesicles, as if non-specifically taken up as part of the fluid phase (Supplementary Fig. 3). These vesicular transport results further demonstrate the importance of 3D culture and imply that in the MVNs, transport of albumin and IgG occurs through physiologically-relevant transcytosis, possibly via different processes.

3.4. Investigation of FcRn-mediated transcytosis

Understanding how particular proteins cross the endothelium is key to inform the design of effective biopharmaceuticals. Next, we applied the MVNs methodology to investigate the transcytosis of albumin and IgG. These proteins constitute, respectively, the first and second major protein constituents of blood plasma, where they are present in a concentration of the order of tens of mg mL^{-1} [37]. Hence, we first considered the effect of perfused mass on transport of these two molecules, increasing the concentration from low to physiologically-relevant concentrations (0.1–10 mg mL^{-1}, Fig. 6a). The effective permeability is found to decrease with increasing concentration, a trend that cannot be explained by a larger luminal oncotic pressure alone. Indeed, the decrease in permeability is non-linear within a concentration range where the oncotic pressure increases linearly with protein mass [37]. Thus, an additional factor must impact the measurement.

One possible explanation for the decrease in permeability with protein concentration is that, contrary to paracytosis, where diffusion through endothelial cell junctions is proportional to the luminal concentration, the process of transcytosis can be saturated. In fact, in the case where fluid and solutes are brought into the cell non-specifically (pinocytosis) and the vesicles may cross to the basal surface, the flux due to transcytosis can be expressed as [38]:

$$J_{trans} = N_v\, V_v\, SA\, \Delta c \quad \text{(Eq. 4)}$$

where N_v is the rate of vesicle formation per area of endothelium and V_v the volume of a single vesicle. The permeability due to transcytosis alone would, therefore, be given by:

$$P = N_v\, V_v \quad \text{(Eq. 5)}$$

In the case of receptor-mediated transcytosis, however, a solute will cross the endothelium only when bound to its receptor, and the permeability relationship takes the form:

$$P = N_v\, V_v\, \frac{c_r}{c_A + K_d} \quad \text{(Eq. 6)}$$

where c_r is the receptor concentration per vesicle, c_A the solute concentration on the apical side, and K_d the solute-receptor dissociation constant (full derivation available as part of the Supplemental Material).

Therefore, as c_A increases, the permeability for the case of receptor-mediated transcytosis decreases. Further, taking the inner vesicle radius as 25 nm (based on SEM imaging in Fig. 5e and in line with previous reports [39]) and N_v as 121 vesicles $\mu m^{-2}\ s^{-1}$ (calculated from the number of vesicles per μm^2 in the MVNs system, 4.84, Fig. 5e, and taking the average luminal-to-basal diffusion time for vesicles across an endothelium that is approximately 500 nm thick as 0.02 s [39]), the decrease in permeability for the two proteins can be fitted by Eq. (5) to yield $c_r = 5.35 \pm 0.38\,\mu M$ and $K_d = 83.43 \pm 6.44\,\mu M$ for albumin, and $c_r = 551 \pm 229\,nM$ and $K_d = 23.86 \pm 12.21\,\mu M$ for IgG. This analysis, which assumes no paracellular transport of the two proteins, suggests that different receptors may be involved in transport of albumin and IgG, and their saturation may decrease the effective permeability measured.

A receptor of particular importance for both albumin and IgG is the neonatal Fc receptor, FcRn. This receptor, expressed in both endothelial and epithelial cells, plays a key role in governing the long half-life of these two serum proteins, by salvaging them from lysosomal degradation upon binding within the acidified endosome [11]. Due to this capability, FcRn has attracted considerable attention as a binding target to extend the half-life of biopharmaceuticals in circulation, thus allowing for less frequent dosing [1]. Here, we confirm that FcRn is expressed in the MVNs and that IgG is more strongly co-localized with this receptor compared to albumin (Fig. 6b), in agreement with what has previously been reported by others in animal models [40]. The recycling of IgG in the MVNs is observed by greater localization of the protein within the endosome rather than the lysosome, a trend also observed for albumin, albeit not significantly (Fig. 6c). In comparison, dextran is not differently localized in either compartment, implying that this molecule is not preferentially salvaged from degradation.

FcRn was also shown to play an important role *in vivo* as a transporter for IgG across epithelia whereby, upon binding, the protein is transported to the opposite side of the cell [41]. Within the endothelium, FcRn-dependent transcytosis is not well understood; previous studies in animal models have reported contrasting results, including no effect on IgG transendothelial distribution after knockdown of FcRn in the mouse brain [42], active transport by FcRn of Fc-conjugated proteins in the bovine retinal endothelium [43], and basal-to-

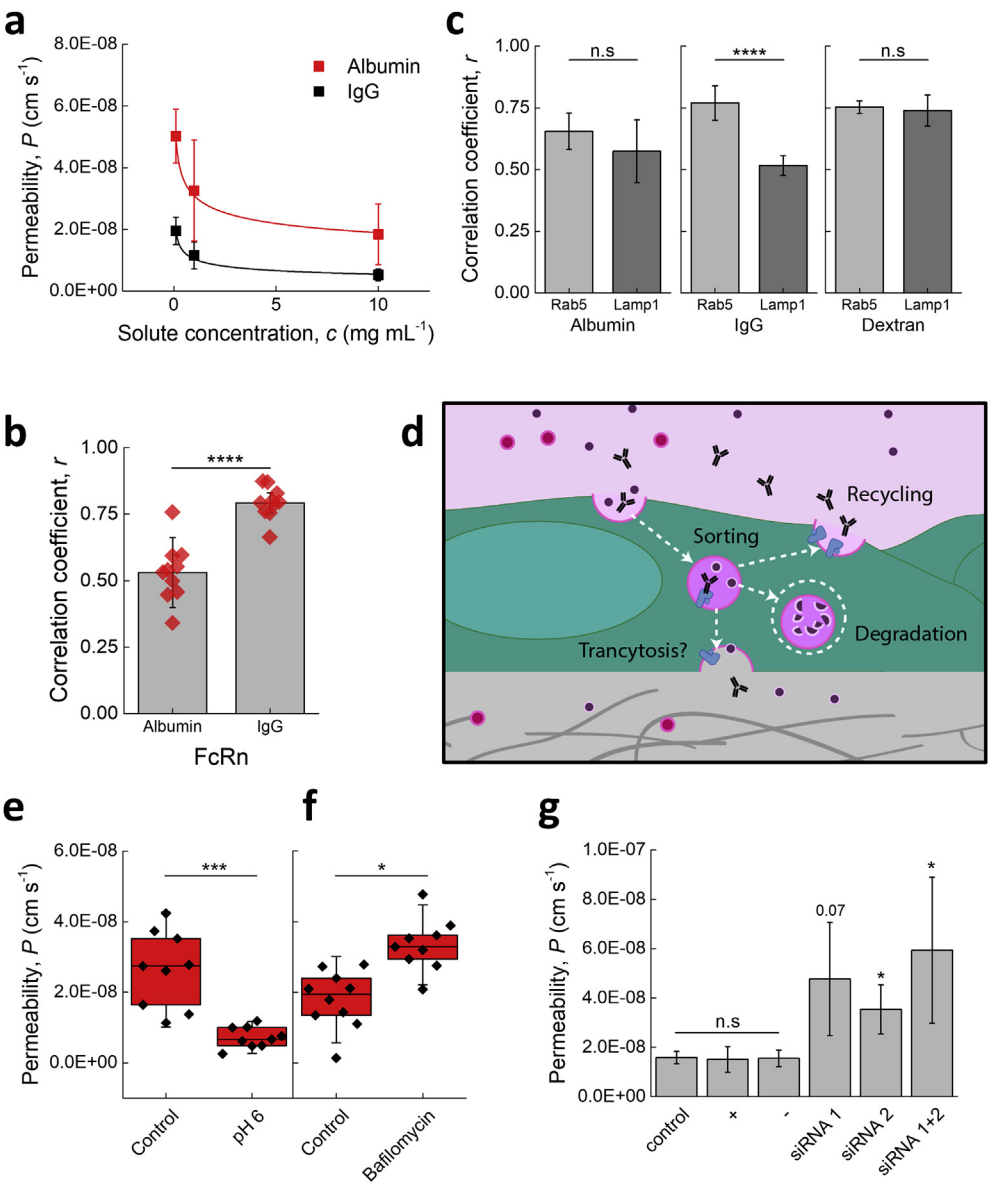

Fig. 6. FcRn antagonizes luminal-to-basal transcytosis of IgG, but not of albumin. (**a**) MVN permeability to albumin and IgG as a function of solute concentration. The curve fits are based on the numerical model for saturation of receptor-mediated transcytosis reported in the text. (**b**) Co-localization analysis of albumin and IgG with FcRn. (**c**) Colocalization of albumin, IgG and 150 kDa dextran with markers for the early endosome (RAB5) and lysosome (LAMP1); $n = 2 \times 5$ measurements. (**d**) Schematic diagram of possible roles of FcRn in endothelial cells. (**e**) MVN permeability to IgG as a function of luminal pH and (**f**) endosome pH. The box and whisker plot represents the outliers that fall within the 25th and 57th percentile; $n = 3 \times 3$ measurements. (**g**) MVN permeability to IgG as a result of FcRn knock-out, compared to control, positive (+), and negative (−) controls. Data portrayed as average and standard deviation; $n = 2 \times 3$. Statistical significance assessed for all data portrayed by student's t-test, *, $p < 0.001$ **, $p < 0.0001$ ***, $p < 0.00001$ ****.

luminal-only transport of IgG in the rat brain [44]. Given the importance that FcRn already holds in the design of biopharmaceuticals, understanding its possible role in IgG transport across a human endothelium holds great potential to tailor the *in vivo* biodistribution of those molecules (Fig. 6d).

In an effort to elucidate FcRn-mediated IgG transport, we first changed the pH in the microenvironment of key binding sites to either increase or decrease the strength of interaction between IgG and FcRn. A decrease in pH to ~6 on the luminal side has been shown to increase binding to FcRn, and so to enhance transcytosis across epithelial layers [45]. In the MVNs, the opposite trend was observed (Fig. 6e) in that transport decreased when IgG was perfused in pH 6 cell culture medium. In contrast, bafilomycin A1 was used to increase the pH within the early endosome, which has been shown to hinder IgG binding to FcRn [46]. Treatment of the MVNs with bafilomycin A1 results in increased permeability to IgG (Fig. 6f). Additionally, we explored the role of FcRn-mediated transcytosis of IgG using siRNA to knock down FcRn in the MVNs, observing an increase in transport of IgG across the endothelium (Fig. 6g). This phenomenon was not also observed with albumin (Supplementary Fig. 4). Consistently, these results suggest that, in the *in vitro* human endothelium MVN model, FcRn does not transport IgG from lumen to matrix. Rather, it may act as an efflux mechanism to remove IgG from the intracellular environment through its recycling action, thus, antagonizing IgG transcytosis.

4. Discussion and conclusions

Precise measurement of protein transcytosis across the endothelium is a critical unmet need for assessing the potential efficacy of novel biotherapeutics. Self-assembly of human endothelial cells into 3D perfusable microvascular networks results in a system that enables these measurements. The MVNs present physiological endothelial attributes that are critical for determining the transendothelial distribution of molecular species *in vivo*. The presence of continuous tight junctions between endothelial cells, as well as a functional glycocalyx, provide a size- and charge-selective barrier to the passage of solutes, demonstrating a significant role for transcytosis in the transport of albumin and IgG under homeostatic conditions. The MVNs outperform conventional transwell systems, where endothelial cells plated on relatively stiff substrates in 2D form non-continuous junctions that allow passage of small and large molecules alike, producing permeability values much larger than those reported in animal models. The MVNs are also superior in their ability to accurately quantify and classify physiological transport pathways.

Leveraging the physiologically-relevant transport properties of the MVNs, we studied the transcytosis of albumin and IgG because of their importance as components in biopharmaceuticals. The ability to interact with FcRn within endothelial cells provides these two proteins, and their fusions, long half-lives in circulation, yet the role of the receptor as an active transendothelial transporter has not been clearly elucidated. Our results suggest that, in the MVNs' human endothelium, FcRn is indeed involved in the transcytosis of IgG, but as an antagonizing agent that diminishes overall transport from the circulation. Albumin was not affected by the presence of FcRn, and its recycling through the receptor is less evident compared to IgG. The localization of albumin within caveolae suggests, instead, possible transport by the receptor gp60, and reveals that the two proteins studied cross the MVNs human endothelium in different ways. It is unclear how, specifically, IgG crosses the endothelium, but the saturation of its transport and greater localization in distinct vesicle types suggests that another receptor may be involved.

Protein-specific mechanisms of paracellular and transcellular exchange can be identified and quantitatively characterized using the 3D MVNs. Such capabilities may be leveraged to investigate, for example, how different binding affinities to FcRn impact transport and recycling, or how smaller biopharmaceuticals such as Fc fragments or peptide antagonists might bypass the size-selective barrier. From a practical point of view, formation of the MVNs within microfluidic devices ensures that relatively small amounts of molecules and reagents may be used, in a reproducible system that allows scaling for industrial applications, such as screening candidate molecules. Ultimately, the superior physiological relevance of transport measurements within the MVNs compared to standard 2D *in vitro* models, as well as the greater spatio-temporal control of the measurement compared to complex animal models, can increase the rate of assessment of biopharmaceuticals to help design molecules with optimized biodistribution properties and, therefore, increased efficacy and safety.

Data availability

The research data for this study is available from the corresponding authors.

Acknowledgements

KH is grateful for partial support from an NSERC fellowship, MRG for support from a Postdoctoral Fellowship with the Canadian Institutes for Health Research, a Detweiler Research Fellowship with the Royal College of Physicians and Surgeons of Canada, and a Dr. Subrata Ghosh Research Fellowship from the University of Calgary. The authors also thank Jeff Lichtman from Harvard University for providing access to SEM facilities, Larry Wienkers for valuable research discussions, and Jordan Whisler and Michelle Chen for useful suggestions related to MVNs formation.

Appendix A. Supplementary data

Supplementary data to this article can be found online at https://doi.org/10.1016/j.biomaterials.2019.05.022.

References

[1] R.E. Kontermann, Half-life extended biotherapeutics, Expert Opin. Biol. Ther. 16 (2016) 903–915.
[2] W. Wang, E.Q. Wang, J.P. Balthasar, Monoclonal antibody pharmacokinetics and pharmacodynamics, Clin. Pharmacol. Ther. 84 (2008) 548–558.
[3] P. Li, Y. Zheng, X. Chen, Drugs for autoimmune inflammatory diseases: from small molecule compounds to anti-TNF biologics, Front. Pharmacol. 8 (2017) 460.
[4] H.O. Alsaab, S. Sau, R. Alzhrani, K. Tatiparti, K. Bhise, S.K. Kashaw, A.K. Iyer, PD-1 and PD-L1 checkpoint signling inhibition for cancer immunotherapy: mechanism, combinations, and clinical outcome, Fron. Pharmacol 8 (2017) 561.
[5] Statista (accessed November 2018), https://www.statista.com/statistics/817593/revenue-forecast-for-global-biologics-market.
[6] L.I. Goulatis, E.V. Shusta, Protein engineering approaches for regulating blood-brain barrier transcytosis, Curr. Opin. Struct. Biol. 45 (2017) 109–115.
[7] M. Tabrizi, G.G. Bornstein, H. Suria, Biodistribution mechanisms of therapeutic monoclonal antibodies in health and disease, AAPS J. 12 (2010) 33–43.
[8] D. Mehta, A.B. Malik, Signaling mechanisms regulating endothelial permeability, APS Physiol. Rev. 86 (2006) 279–367.
[9] K. Haase, R.D. Kamm, Advances in on-chip vascularization, Regen. Med. 12 (2017) 285.
[10] B. Godin, E. Touitou, Transdermal skin delivery: predictions for humans from in vivo, ex vivo and animal models, Adv. Drug Deliv. Rev. 59 (2007) 1152–1161.
[11] D.C. Roopenian, S. Akilesh, FcRn: the neonatal Fc receptor comes of age, Nat. Rev. Immunol. 7 (2007) 715–725.
[12] J.A. Whisler, M.B. Chen, R.D. Kamm, Control of perfusable microvascular network morphology using a multiculture microfluidic system, Tissue Eng. C Methods 20 (2014) 543–552.
[13] S. Nitta, T. Ohnuki, K. Ohkuda, T. Nakada, N.C. Staub, The corrected protein equation to estimate plasma colloid osmotic pressure and its development on a nomogram, Tohoku J. Exp. Med. 135 (1981) 43–49.
[14] J.R. Levick, C.C. Michel, Microvascular fluid exchange and the revised Starling principle, Cardiovasc. Res. 87 (2010) 198–210.
[15] J. Schindelin, I. Arganda-Carreras, E. Frise, V. Kaynig, M. Longair, T. Pietzsch, S. Preibisch, C. Rueden, S. Saalfeld, B. Schmid, J.Y. Tinevez, D.J. White, V. Hartenstein, K. Eliceiri, P. Tomancak, A. Cardona, Fiji: an open-source platform for biological-image analysis, Nat. Methods 9 (2012) 676–682.
[16] O. Kedem, A. Katchalsky, Thermodynamic analysis of the permeability of biological membranes to non-electrolytes, Biochem. Biophys. Acta 27 (1958) 229–246.
[17] I.M. Braverman, The cutaneous microcirculation, J. Investig. Dermatol. Symp. Proc. 5 (2000) 3–9.
[18] E. Toyota, K. Fujimoto, Y. Ogasawara, T. Kajita, F. Shigeto, T. Matsumoto, M. Goto, F. Kajiya, Dynamic changes in three-dimensional architecture and vascular volume of transmural coronary microvasculature between diastolic- and systolic-arrested rat hearts, Circulation 105 (2002) 621–626.
[19] S.A. Skinner, P.E. O'Brien, The microvascular structure of the normal colon in rats and humans, J. Surg. Res. 61 (1996) 482–490.
[20] W. Zhan, D.Y. Arifin, T.K. Lee, C.H. Wang, Mathematical modelling of convection enhanced delivery of carmustine and paclitaxel for brain tumour therapy, Pharm. Res. (N. Y.) 34 (2017) 860–873.
[21] B. Amsden, An obstruction-scaling model for diffusion in homogeneous hydrogels, Macromolecules 32 (1999) 874–879.
[22] A. Siflinger-Birnboim, P.J. del Vecchio, J.A. Cooper, F.A. Blumenstock, J.M. Shepard, A.B. Malik, Molecular sieving characteristics of the cultured endothelial monolayer, J. Cell. Physiol. 132 (1987) 111–117.
[23] S.M. Albelda, P.M. Sampson, F.R. Haselton, J.M. McNiff, S.N. Mueller, S.K. Williams, A.P. Fishman, E.M. Levine, Permeability characteristics of cultured endothelial cell monolayers, J. Appl. Physiol. 64 (1988) 308–322.
[24] B.K. Lal, S. Varma, P.J. Peppas, R.W. Hobson, W.N. Duran, VEGF increases permeability of the endothelial cell monolayer by activation of PKB/akt, endothelial nitric-oxide synthase, and MAP kinase pathways, Microvasc. Res. 62 (2001) 252–262.
[25] I. Bischoff, M.C. Hornburger, B.A. Mayer, A. Beyerle, J. Wegener, R. Furst, Pitfalls in assessing microvascular endothelial barrier function: impedance-based devices versus the classic macromolecular tracer assay, Sci. Rep. 6 (2016) 23671.
[26] E.M. Renkin, Multiple pathways of capillary permeability, Circ. Res. 41 (1977) 735–743.
[27] W. Yuan, Y. Lu, M. Zeng, B.M. Fu, Non-invasive measurement of solute permeability in cerebral microvessels of the rat, Microvasc. Res. 77 (2009) 166–173.
[28] M.D. Onken, O.L. Mooren, S. Mukherjee, S.T. Shahan, J. Li, J.A. Cooper, Endothelial monolayers and transendothelial migration depend on mechanical properties of the substrate, Cytoskeleton 71 (2014) 695–706.
[29] Y.I. Wang, H.E. Abaci, M.L. Shuler, Microfluidic blood-brain barrier model provides in vivo-like barrier properties for drug permeability screening, Biotechnol. Bioeng. 114 (2017) 184–194.
[30] M. Dellian, F. Yuan, V.S. Trubetskoy, V.P. Torchilin, R.K. Jain, Vascular permeability in a human tumour xenograft: molecular charge dependence, Br. J. Canc. 82 (2000) 1513–1518.
[31] J.M. Tarbell, L.M. Cancel, The glycocalyx and its significance in human medicine, J. Intern. Med. 280 (2016) 97–113.
[32] R.K. Jain, Transport of molecules across tumor vasculature, Cancer Metastasis Rev. 6 (1987) 559–593.
[33] H.H. Lipowsky, L. Gao, A. Lescanic, Shedding of the endothelial glycocalyx in arterioles, capillaries, and venules and its effect on capillary hemodynamics during inflammation, Am. J. Physiol. Heart Circ. Physiol. 301 (2011) H2235–H2245.
[34] T.S. Reese, M.J. Karnovsky, Fine structural localization of a blood-brain barrier to exogenous peroxidase, J. Cell Biol. 37 (1967) 207–217.
[35] M. von Zastrow, B.K. Kobilka, Antagonist-dependent and -independent steps in the mechanism of adrenergic receptor Internalization, J. Biol. Chem. 269 (1994) 18448–18452.
[36] C. Tiruppathi, W. Song, M. Bergenfeldt, P. Sass, A.B. Malik, Gp60 activation mediates albumin transcytosis in endothelial cells by tyrosine kinase-dependent pathway, J. Biol. Chem. 272 (1997) 25968–25975.
[37] S.Y. Yuan, R.R. Rigor, Regulation of Endothelial Barrier Function, Morgan & Claypool Life Science, San Rafael, CA, 2010.
[38] S. Chien, S. Weinbaum, Vesicle transport in arterial endothelium and the influence of mechanical factors on macromolecular permeability, J. Biomech. Eng. 103 (1981) 186–196.

[39] S. Weinbaum, C.G. Caro, A macromolecule transport model for the arterial wall and endothelium based on the ultrastructural specialization observed in electron microscopy studies, J. Fluid Mech. 74 (1976) 611–640.
[40] K.M. Knudsen Sand, M. Bern, J. Nilsen, H.T. Noordzij, I. Sandlie, J.T. Andersen, Unraveling the interaction between FcRn and albumin: opportunities for design of albumin-based therapeutics, Front. Immunol. 5 (2015) 682.
[41] E.S. Ward, S.C. Devanboyina, R.J. Ober, Targeting FcRn for the modulation of antibody dynamics, Mol. Immunol. 67 (2015) 131–141.
[42] L. Abuqayyas, J.P. Balthasar, Investigation of the role of FcγR and FcRn in mAb distribution to the brain, Mol. Pharm. 10 (2013) 1505–1513.
[43] H.L. Deissler, G.K. Lang, G.E. Lang, Neonatal Fc receptor FcRn is involved in intracellular transport of the Fc fusion protein aflibercept and its transition through retinal endothelial cells, Exp. Eye Res. 154 (2017) 39–46.
[44] P.R. Cooper, G.J. Ciambrone, C.M. Kliwinski, E. Maze, L. Johnson, Q. Li, Y. Feng, P.J. Hornby, Efflux of monoclonal antibodies from rat brain by neonatal Fc receptor, FcRn. *Brain Res.* 1534 (2013) 13–21.
[45] C.A. Castro Jaramillo, S. Belli, A.C. Cascais, S. Dudal, M.R. Edelmann, M. Haak, M.E. Brun, M.B. Otteneder, M. Ullah, C. Funk, F. Shuler, S. Simon, Towards in vitro-to-in vivo translation of monoclonal antibody pharmacokinetics: application of a neonatal Fc receptor-mediated transcytosis assay to understand the interplaying clearance mechanism, mAbs 9 (5) (2017) 781–791, https://doi.org/10.1080/19420862.2017.1320008.
[46] N.A. Goebl, C.M. Babbey, A. Datta-Mannan, D.R. Witcher, V.J. Wroblewski, K.W. Dunn, Neonatal Fc receptor mediates internalization of Fc in transfected human endothelial cells, Mol. Biol. Cell 19 (2008) 5490–5505.